The prelimbic cortex arbitrates memory-guided conflict resolution

Steve Ramirez

dvsteve@bu.edu

Department of Psychological and Brain Sciences, The Center for Systems Neuroscience, Boston University https://orcid.org/0000-0002-9966-598X

Albit Caban-Murillo

Department of Psychological and Brain Sciences, The Center for Systems Neuroscience, Boston University

Michelle Surets

Department of Psychological and Brain Sciences, The Center for Systems Neuroscience, Boston University

Celine Chien

Department of Psychological and Brain Sciences, The Center for Systems Neuroscience, Boston University

Marun Kauffman

Department of Psychological and Brain Sciences, The Center for Systems Neuroscience, Boston University

sarah Park

Department of Psychological and Brain Sciences, The Center for Systems Neuroscience, Boston University

Biological Sciences - Article

Keywords:

Posted Date: July 12th, 2024

DOI: https://doi.org/10.21203/rs.3.rs-4618930/v1

Additional Declarations: There is **NO** Competing Interest.

Abstract

Balancing reward and avoidance to produce an adaptive behavior is a critical aspect of conflict resolution. Here, we investigated how mice balance reward-seeking and avoidance during memory-guided conflict resolution. Mice were trained to combine the drive to approach a reward and avoid a foot shock without compromising either goal. During training, mice learn that a light cue signals the availability of reward and an auditory cue signals the onset of a foot shock which they can avoid by stepping onto a platform. During testing, the light and auditory cues are delivered simultaneously, creating a conflict between reward-seeking and punishment avoidance. Our results demonstrate that mice learn to flexibly accommodate behavioral drives to maximize rewards while avoiding the foot shock. We then leveraged a whole-brain tissue clearing approach to identify sex-specific whole-brain activity profiles, and specifically identified the PL as a central hub. Using calcium imaging, we found PL activity signals task variables and predicts successful conflict resolution. Finally, silencing PL engrams disrupts the balance between reward seeking and avoidance behaviors. These findings reveal the PL's mechanistic role in guiding behavioral flexibility in a sex-specific manner.

Introduction

Conflict resolution often requires balancing behavioral drives including threat avoidance and the pursuit of reward–two major behavioral motivators whose impairments are hallmarks of neuropsychiatric disorders such as PTSD and addiction [1-3]. For instance, sustained threat responses can be at odds with the pursuit of rewarding activities and may lead to decreased social behaviors and anhedonia. In contrast, excessive reward-seeking in the face of threat risks self-preservation and can become maladaptive. Dysfunction of the human anterior cingulate cortex (ACC) and its proposed rodent analog prelimbic cortex (PL) are known to underlie core behavioral features of impairments to the balancing of behavioral drives across species [4-6].

Prior studies have described PL to have a critical role in the consolidation of threatening and rewarding memories [7,8]. Moreover, recent studies have shown that activity in PL is correlated to threat avoidance behaviors and reward seeking [9-11]. Suppression of PL activity in a probabilistic reward decision-making task disrupts how past outcomes inform future decisions [12]. Still, it remains unknown whether or not PL activity is necessary to support conflict resolution when opposing drives are pitted against each other. In terms of cellular correlates, a sparse population of neurons active during an experience are thought to store memory-related information. The ensemble of neurons that are concomitantly active and store a given experience is provisionally termed an “engram” [13-15]. Previous studies show engrams store memory conducive to reward seeking and threat responsive behaviors [16-18]. In the medial prefrontal cortex (mPFC), studies have shown engrams store fear and reward memories and are subsequently necessary for memory retrieval [8, 19]. Moreover, engrams are spread throughout the brain and can generate flexible behavioral responses [18, 20-21]. Work in the hippocampus has shown engrams storing memories of reward and fear memories recruit genetically and anatomically distinct groups of cells [22],

though most engram studies to date have focused on how engrams of a single valence are conducive to behavior. In general, how multiple engrams of distinct valences interact to guide behavior—and in particular, how the PL may recruit reward-seeking and threat-avoidance engrams to enable conflict resolution—

has remained relatively unknown.

Here we adapt a recently developed decision-making task that allows animals to strategically combine seeking reward and avoidance of a foot shock without compromising either goal [23]. This conflict is presented across days to allow animals to develop a conflict resolution strategy that flexibly accommodates both drives. As PL ensembles have a role in reward seeking and avoidance of threat independently, we hypothesized the PL would be a critical arbitrator for conflict resolution between reward seeking and threat avoidance. Leveraging brain-wide cFos immunostaining and graph-theoretical approaches we show that the PL is recruited across sexes during memory-guided conflict resolution and is uniquely poised to arbitrate between motivational drives. Furthermore, using bulk calcium imaging we show PL activity is modulated by both reward seeking and avoidance during our task. Critically, PL activity predicted if mice would correctly arbitrate motivational drives during the task. Finally, by selectively silencing reward seeking and avoidance engrams within PL we show that animals become unable to flexibly accommodate behavior to resolve conflict. Our results thus point to a causal role of the PL as an arbitrator of memory-guided behavior during conflict resolution.

Results

Mice learn to balance behavioral drives across training

When repeatedly confronted with the same choice, animals develop strategies to maximize rewards and minimize costs. Balancing reward seeking and avoidance of threats is critical, especially when these drives conflict. To study how memory guides conflict resolution, water restricted mice were trained in a decision making paradigm that sets the drive to seek reward against the drive to avoid a footshock [23]. First, mice were trained to associate a 30s light-cue with reward availability (e.g. water) by poking at a noseport (Reward training). Next, mice were trained to associate a 30s tone-cue with a footshock delivered during the final 3s (Interleaved avoidance training). In this task, mice learn to avoid the footshock by stepping into a platform before a shock is delivered. one-cue trials were interleaved with light-cue trials and separated by 60s intertrial interval (ITI) to promote exploration of the behavioral chamber. Finally, to create a conflict between reward seeking and the avoidance of the footshock, both 30 cues are co-presented (Conflict training) **(Fig 1A)**. During reward training, time poking during the light-cue increased and outside the light-cue decreased across days. During avoidance training, mice increased the time they spent in the platform during the tone-cue, while continuing to spend increased time poking during the light-cue **(Fig 1B)**. Both males and female mice significantly decrease the time they spend on the platform and poking for reward across training **(Fig 1C-D)**. Strategically, mice can display 3 behavioral phenotypes across conflict training: Stay on the platform the entirety of the trial

(Avoiding), poke for reward the entirety of the trial and receive a footshock (Seeking), or poke for reward early and step into the platform before the footshock is delivered (Timing) **(Fig 1E)**. Across days, mice increased the percent of trials in which they chose a Timing strategy, while decreasing the trials in which they chose a Seeking or Avoiding strategy **(Fig 1F)**. However, male mice chose the Timing strategy more and the Seeking and Avoiding strategies less across training **(Fig 1G-I)**. Using a Markov-Chain model to better understand the choice of strategies in the current trial given the past trial, we observed that mice consistently chose the Timing strategy. Further, after trials in which animals chose less optimal strategies like Seeking or Avoiding which force animals to either receive a shock or nor receive reward, mice tended to correct the behavior in the following trial to Timing **(Figure 1J)**. Taken together, across training mice learn that to solve a conflict between the drive to seek reward and the drive to avoid a footshock, they poke for reward early and avoid the shock later. This learning exhibits sex dependent differences, where male mice chose Timing more across trials and days than female mice.

Brain-wide cFos profiles during conflict resolution

To catalog the brain regions recruited to balance the drive to poke for reward and the drive to avoid a footshock, we measured the activity dependent gene c-Fos across 120 brain regions. After a conflict session in which mice displayed a Timing strategy, all subjects were timed perfused 90 minutes later. As a control, a group of mice did not receive any training but were introduced to the same context and number of cues as the experimental group **(Fig 2A)**. Following time perfusion, tissue underwent whole organ clearing, immunohistochemistry, and light-sheet microscopy, allowing the quantification of whole-brain cFos density **(Fig 2B)**. The difference in cFos density between groups was obtained for males and females **(Fig 2C-N)**. Among the regions with significant increases in cFos density in males and females are the Anterior Cingulate Area (ACA), the Prelimbic cortex (PL), and hippocampal areas CA1, CA2, and CA3. For males, the Medial Hypothalamus (MH), Inferior Colliculus (IC) showed a decrease in cFos density, while the Subiculum (SUB) showed an increase compared to controls. For Females, more overall regions showed a increase in cFos like the Orbitofrontal area (ORB), Agranular Insula (AI), Dentate Gyrus (DG), Nucleus Accumbens (ACB), the dorsal and veteran regions of the striatum (STRd and STRv), the Lateral Hypothalamus (LH), and the Periaqueductal gray (PAG). Additionally, the Locus Ceruleus (LC) had a decrease in cFos density in males and an increase in females. Overall, males and females recruit both overlapping and distinct regions during conflict resolution.

We next employed network analysis to quantitatively understand the key regions recruited during conflict resolution and their correlative roles within the brain network. Complex network analysis leverages a graph-theoretical approach to study real-life biological networks. By analyzing network measures we first detected features that reflect functional segregation and integration, resilience, and detect central nodes (Hubs) to the network [24-25]. Functional networks were constructed from cFos density cross-correlations **(Fig 3A-B)** [18,26]. Here, each individual brain region is considered a node while the correlation in cFos density between regions is considered an edge and its value the relative weight of that edge. **(Fig 3C)**. We identified central hubs for both the male and female networks **(Fig 3D)**. For males, we detected a subset of hubs known to be implicated in valence processing (e.g. PVT and CEA), others known to

regulate reward seeking and defensive behaviors (e.g. MH and VMH), and others associated with memory and attention (e.g. CA1, DR, LC, and RE). For females, a subset of hubs included memory associated areas (e.g. DG, SUB, and PAR), areas associated with goal directed behavior (e.g. ACA, AI, and ACB), and areas that regulate defensive and reward seeking behaviors (TH). Both male and female overlapping hubs include executive function (PL), sensory integration (RSP), valence processing (LA), and regulation of defensive and reward seeking behaviors (HY). Between all four overlapping hubs, the PL had the highest relative values across all network measurements, hence the highest theoretical influence in the network **(Fig 3E)**. This data points to males and females recruiting different brain regions in order to effectively balance behavioral drives during conflict resolution, but critically converging in the recruitment of the PL.

Neural correlates of memory-guided conflict resolution

The PL has been implicated in reward seeking behaviors, active threat responses, and decision-making [9,11-12]. Accordingly, we next virally expressed GCaMP6f in PL neurons and recorded bulk fluorescence on the last day of training to observe if PL activity correlated with our task variables **(Fig 4A-C)**. We found a higher baseline fluorescence prior to the trial start and lower during the early periods of the trial predicted if an animal would choose a Timing strategy **(Fig 4D-E),** suggesting a specific neural state shift is required to drive the Timing strategy. Changes in baseline fluorescence after the trial did not reflect the strategy chosen **(Fig 4F)**. PL neurons signaled cue onset in both males and females, however only in males did PL neurons only signal cue-onset in correct trials **(Fig 4G-J)**. Similarly, poking was signaled by males and females with an increase in fluorescence prior to the poke and a decrease in fluorescence after the poke. Interestingly, only male PL neurons signaled more strongly the onset of a rewarded poke during Timing trials than unrewarded pokes **(Fig 4K-N)**. PL neurons signaled the onset of avoidance by an increase in fluorescence prior to the mouse mounting the platform which was sustained while on the platform. While both male and female mice exhibited significant increases in activity prior to and during the platform mount, only male mice signaled his mount differently than mounts outside of the trial **(Fig 4O-R)**. Importantly, both male and female mice signal the light and tone cues, and behavioral variables similarly when not under conflict **(Fig S2)**. Taken together, the PL of male mice accurately distinguishes between cues and behavioral variables under conflict conditions.

PL reward seeking and avoidance engrams are critical for Timing

To test whether PL engrams processing a reward-seeking or avoidance memory are necessary for Timing, we leveraged an activity dependent labeling strategy to express an inhibitory Designer Receptors Exclusively Activated by Designer Drugs (DREADDs). This approach restricts labeling in a dox-dependent manner, allowing for chemogenetic silencing of the tagged experience only **(Fig 5A-B)**. A day prior to the start of conflict training, animals underwent an additional reward, avoidance or neutral cage session in which cells active were tagged. Chemogenetic silencing of both the reward seeking and avoidance engrams in males disrupted their ability to use the Timing strategy compared to mCherry controls and neutral cage engram silencing **(Fig 5C-G)**. Additionally, silencing of the reward seeking engram biased

animals towards the Avoiding strategy. Similarly, silencing of the reward seeking and avoidance engrams in females disrupted their ability to use the Timing strategy compared to mCherry and neutral tagged controls **(Fig 5H-L)**. In females, both silencing the reward seeking and avoidance engrams biased mice into using an Avoiding strategy. Our data demonstrate that PL engrams are essential for balancing reward seeking and avoidance of punishment under conflict in both males and females. Moreover, silencing these engrams does not hinder the encoded behavior itself but disrupts the adaptive balancing between the two behaviors.

Discussion

Here we show that male and female mice learn to balance reward-seeking and avoidance of a footshock to guide conflict resolution. While male mice balanced these drives in a timing strategy earlier in training, both sexes implemented the timing strategy by the end of training. We next demonstrate through whole-brain cFos density that the PL is recruited during this timing behavior and in a network is positioned to be critical for information processing. Furthermore, we show PL activity correlates with task variables and contains engrams necessary for the adequate balancing of behavioral drives. Together, our data point to PL dynamics and engrams as arbitrators guiding behavioral flexibility under conflict.

By leveraging brain-wide cFos expression patterns we characterized whole-brain activity profiles recruited during conflict resolution. Critically both male and females exhibited high cFos expression in prefrontal and hippocampal areas, suggesting they are recruited for conflict resolution. Previous findings have shown hippocampal areas harbor both reward and fear engrams, and their selective reactivation is sufficient to guide behavior [22]. Moreover, the hippocampal area CA1 and CA3 have been shown to be necessary for approach-avoidance conflict resolution [27-28]. Similarly, prefrontal areas have been observed to be necessary for reward-cue associative learning, platform mediated avoidance, learning task rules, and cognitive control [10, 29-33]. Interestingly, females having higher cFos expression in striatal areas, which have been observed to support cue-responses and behavioral inhibition, and may suggest a higher demand for behavioral inhibition, as female mice are more likely to keep reward-seeking than to stop and avoid [34, 35]. To further catalog ‘hubs’ recruited for conflict resolution we employed a graph-based theoretical approach [25]. Here males had more subcortical hubs than females suggesting sex-speciffic processing streams may be recruited at a network level to achieve behavioral flexibility [36-39]. However, the PL was among the few areas in which recruitment was conserved across sex-specific networks. Interestingly, the PL projects to many of the other sex specific hubs [40], suggesting it might be accessing different brain wide processing streams across sexes.

Next, using bulk calcium imaging in PL we identified activity correlated to task variables including cue onset, poking, and avoiding, and activity predictive of the employment of a timing strategy. We observed activity prior to a trial start and during the early portion of the task predicted if an animal would be able to stop reward seeking and avoid the footshock. Previous studies have shown mPFC activity is required for initiating and terminating actions [12], and represents ‘self’ states [41], suggesting PL higher activity prior

to a trial may reflect a unique behavioral state that promotes behavioral flexibility. We observed neural correlates of cue-onset, reward seeking and avoiding during conflict training and prior to, when there is no conflict between drives. These correlates have previously been characterized at a single cell level for reward seeking and platform mediated avoidance [9, 11, 42]. Curiously, while prior studies have characterized single cell level firing increases and decreases to reward seeking and platform mediated avoidance, respectively [9, 11], we observe that at a global level activity decreases for reward-seeking and increases for avoidance. Recently, a complementary study observed a decrease in the spontaneous activity of glutamatergic neurons to correlate with persistent reward seeking and risk taking [43], this is in line with our findings showing a decrease in global activity during the reward seeking portion of a trial. Importantly, while the PL in male and females signaled behavioral and context variables in our experiments, only in males could we distinguish trial outcome at the cue-onset, and behavior during timing trials was uniquely represented in population activity pointing to sex-specific degrees of recruitment of the PL to represent behavioral relevant information. Despite representational differences, by selectively labeling and silencing reward-seeking or avoidance engrams in PL we show these are critical for the balancing of behaviors required by the timing strategy across sexes. Previous work has shown engrams to drift and reorganize to support novel information [44, 45], supporting the notion of these reward-seeking or avoidance engrams in PL reorganizing across learning to drive the behavioral repertoire required for the timing strategy, rather than solely representing one behavioral drive.

Our behavioral findings show all mice learn to use the timing strategy to maximize reward consumption while minimizing punishment received. In rats, recent findings suggest that reward or avoidance-oriented phenotypes emerge when the drive for reward seeking and avoidance of threat are pit against each other [23, 43]. Interestingly, when given sufficient time to learn, one study observed mice indeed learn to resolve conflicts in a way that maximizes reward [46]. Furthermore, we show a sex difference in conflict resolution, where female mice rely less on a timing strategy and are more likely to risk receiving a footshock throughout training. While prior studies have observed female mice to display various threat avoidant behaviors, to express high levels of freezing after fear conditioning, and to have higher risk assessment [23, 47-48], our data is consistent with studies showing females to have a higher reward sensitivity [49]. The drives to seek reward and avoid punishment are in conflict often in our lives. How individuals flexibly adapt to this conflict allows making decisions that maximize positive outcomes while minimizing negative consequences, showcasing their ability to navigate complex and dynamic environments effectively. However, this ability can be significantly hindered by anxiety and addiction disorders where a skewed prioritization of either reward seeking or avoidance of danger results in maladaptive behaviors. Our findings highlight the importance of studying sex differences in more complex tasks that mimic the motivational conflicts commonly encountered by humans. Critically, our study underscores the pivotal role of the PL in mediating behavioral flexibility and balancing reward-seeking and avoidance drives, highlighting its potential involvement in disorders characterized by impaired conflict resolution.

Materials and Methods

Subjects:

One hundred and seven experimentally naive, male and female c57bl/6 mice (2-3 months of age) from Charles River Laboratories were used. Animals were housed in groups of up to 5 mice per cage. The animal vivarium was maintained on a 12:12-hour light cycle (lights on at 07:00). Mice were water deprived one day prior to training, with all animals receiving at least 1 mL of water per day throughout the entire duration of being water deprived. Animals were provided with ad-libitum access to food, with mice in engram-tagging groups being placed on a doxycycline (Dox) diet prior to surgery. Mice were given at least 14 days after surgery to recover prior to the start of any behavior. Dox was replaced with standard mouse chow 24 hours prior to behavior to open a time window of activity-dependent labeling (Liu 2013). The colony room was maintained on a 12-hour light/dark cycle. Behavior was run under red light and testing occurred at a consistent time to avoid temporal activity confounds. Experimental procedures were approved by IACUC.

Stereotaxic Surgery:

Mice were anesthetized using isoflurane (inducted at 4%, lowered to 2-3% for the maintenance during surgery) and placed in the stereotaxic frame atop a heating pad to maintain body temperature. Hair was removed with a hair removal cream and ophthalmic ointment was generously applied to both eyes to prevent corneal drying. The surgical site was cleaned with alternating application of betadine and ethanol. An incision was made with a scalpel to expose the skull. The brain was then zeroed relative to the skull, and the following coordinates were used: 2.0 anteroposterior (AP), 0.3 mediolateral (ML), and -1.8 dorsoventral (DV) for the PL.

Mice were bilaterally injected with 300 ul of a given viral vector at a rate of 120 ul/min. When performing injections, the needle was lowered to -2.05 DV and left to rest for 3 minutes prior to being pulled up to -2.0 and injected. Then, the needle remained at -2.0 for five minutes before being removed. For photometry, mice received unilateral optic fiber implants 0.1 mm above the site of infusion (Doric Lenses). The implant was secured to the skull with a layer of adhesive cement (C&M Metabond) followed by multiple layers of dental cement (Stoelting). Following surgery, mice were injected with a 0.1mg/kg intraperitoneal (IP) dose of buprenorphine. Virus was given at least 14 days to express prior to the start of the experiment.

Viral vectors:

For overlap experiments, pAAV9-cFos-tTA, pAAV9-TRE-eYFP were constructed as previously described (Ramirez et al., 2015). AAV9-c-Fos-tTA was combined with AAV9-TRE-eYFP (UMass Vector core) prior to injection at a 1:1 ratio. Similarly, for silencing experiments, AAV9-c-Fos-tTA was combined with AAV9-TRE-HM4Di or AAV9-TRE-mCherry (UMass Vector core) prior to injection at a 1:1 ratio. For photometry experiments, AAV9-hsyn-GCaMP6f (AddGene) was used.

Behavior:

Training was conducted in Med Associates operant conditioning boxes controlled by Trans V software. A dispenser with 10% sucrose water connected to a nose port was located at one end of the chamber, along with a light and speaker. Prior to training, mice were placed on water deprivation to increase their motivation to obtain reward. Mice first underwent one-to-one water training, in which the light was constantly on and they could freely gain access to sucrose water at any point during the 30 min session by performing a nose poke. Animals went through three days of one-to-one training and all got at least one hundred rewarded nose pokes within the 15 minute trial duration before advancing in training. In the Reward training phase, sucrose water was no longer freely available during the task but rather during select periods indicated by the light cue. When the light cue turned on, the mouse then had 30 seconds in which it could poke for sucrose water. After time was up, sucrose water was unavailable for the 60s inter-trial interval (ITI). After five days of Reward training, mice underwent three days of Interleaved Avoidance training. Here, light-cue trials were interleaved with tone-cue trials, separated by a 60s ITI. Mice learned, a 30s tone-cue terminated with a footshock (0.4 mA). Mice could avoid this footshock by stepping into a nearby plastic platform which was located opposite to the reward port to ensure mice could not get reward while on the platform. Following, mice underwent Conflict training for seven days. Where the tone and light cues were combined in order to create a motivational conflict.

Behavioral acquisition:

Video data throughout training was taken using GoPro cameras. For behavioral curves, behavior was manually annotated and cross-verified. For photometry and silencing experiments, behavior was analyzed by manually annotating and using video tracking software (EthoVision).

Histology:

Mice were sacrificed and perfused transcardially with phosphate buffered saline (PBS) followed by 4% paraformaldehyde (PFA) in PBS. Brains were then extracted and stored in PFA for at least 24 hours. Brains were sliced coronally at increments of 50 um using a vibratome and stored at 4°C in 0.01% sodium azide in PBS. When staining was performed for cFos overlaps, slices were washed with PBS for 3 washes of 10 minutes, then blocked on a shaker for 1.5 hours using 5% bovine albumin serum (BSA). Slices were then moved to wells with primary antibodies in 1% BSA (1:1000 rabbit anti-cFos [Abcam] and chicken anti-GFP [ThermoFisher]) and allowed to incubate for 48 hours on a shaker at 4°C. Two days later, slices were washed in PBS for 3 washes of 5 minutes each, then were allowed to incubate for 1.5 hours with secondary antibodies in 1% BSA (1:200 Alexa Fluor 555 goat anti-rabbit [ThermoFisher] and Alexa Fluor 488 goat anti-chicken [ThermoFisher]) before being washed with PBS once more for 4 washes of 10 minutes each. For silencing experiments, a different set of primary antibodies (1:1000 each of guinea pig anti-RFP [SySy] and rat anti-cFos [Millipore]) and secondary antibodies (1:200 each of Goat Anti-Rat 488 Alexa Fluor [Abcam] and Goat anti Guinea Pig 555 Alexa Fluor [Abcam]) was used. Slices were then mounted on slides using Vectashield HardSet Mounting Medium with DAPI (Vector Laboratories, Inc), coverslipped, and dried at room temperature overnight before being moved into the fridge.

LifeCanvas Technologies

Brains for brain-wide cFos analyses were stored in PFA for 24 h after perfusion and extraction. They were then stored in 0.02% sodium azide solution before being sent to LifeCanvas Technologies for brain-wide cFos detection. Once there, brains undergo a series of preservation and clearing steps using SHIELD and SmartClear Pro technology, respectively. Next, the samples are washed and prepped for organ-scale immunolabeling using SmartLabel reagents. Samples are batch labeled in 3.5 µg rabbit anti-cFos per brain using SmartBatch and are left to incubate for roughly 18 h. Then, samples undergo a series of washes and fixation steps over4 • days before being incubated in secondary solutions. Finally, brains are mounted in agarose+EasyIndex solution for image preparation. Brain-wide images are acquired using a SmartSPIM microscope equipped with a 3.6× objective with a 1.8 µm×1.8 µm pixel size and a z-step size of 4 µm. The axial resolution of the images is <4.0 µm. The samples are imaged using two channels: 488 nm (autofluorescence/NeuN) and 642 nm (cFos). The autofluorescence channel is used to align the images to the Allen Brain Atlas (Allen Institute for Brain Science: https://portal.brain-map. org/). LifeCanvas Technologies carries out this alignment process in two phases. The first phase is an automated process that samples 1020 atlas-aligned reference samples for each brain sample using a variety of SimpleElastix warping algorithms. An average alignment was computed for all other intermediate images. To confirm the efficacy of the alignment algorithm, the second phase uses a custom Neuroglancer interface (Nuggt: https://github.com/chunglabmit/nuggt) for manual confirmation of the automated alignment algorithm. Once the images were aligned, cell populations were then mapped onto the atlas for region-specific quantification. LifeCanvas Technologies developed a custom convolutional neural network using the TensorFlow Python package. Cell detection was performed by two networks in sequence. Once the cells were aligned and quantified, cFos data were aggregated into .csv files and sent back to the Ramirez group for further analyses as described below.

Image Acquisition and Analysis:

We acquired images using an LSM-800 confocal microscope with a 10x objective lens (Carl Zeiss AG). Images were captured either manually with no focus strategy or were automated using the software autofocus feature in Zen Blue (ver. 2.3) to detect the most intense fluorescent pixels within the defined z-stack. Using ImageJ, one composite image was created per slice using maximum projections of each channel. Overlapping cells between different channels in composite were analyzed using the QuPath software.

Fiber photometry acquisition:

A 470-nm LED (Neurophotometrics FP3002) delivered an excitation wavelength of light to PL neurons expressing GCaMP6f via a single fiber optic implant. The emitted 530-nm signal from the indicator was collected via this same fiber and patch cord (Doric Lenses), spectrally-separated using a dichroic mirror, passed through a series of filters, and was focused on a scientific camera. Isosbestic signals were simultaneously captured by alternating excitation with 415-nm LED to dissociate motion, tissue autofluorescence, and photobleaching from true changes in fluorescence. All wavelengths were

interleaved and collected simultaneously using Bonsai interfacing with the Neurophotometrics system. The sampling rate for the calcium signals was 10 Hz per channel.

Chemogenetic Manipulation:

Deschloroclozapine (DCZ) was used as the ligand for selectively activating the injected DREADDs (designer receptors exclusively activated by designer drugs). DCZ was made within 24 hours of experimental use. Doses were administered to be equivalent to 1 ug/kg per animal and were prepared as previously described [50]. Administration of DCZ was performed 20 minutes prior to beginning of behavior.

Behavioral analysis:

Behavioral analysis was performed using custom code in Python 3.9 and Prism. For calculating time spent in the avoidance zone, we delineated the platform zone utilizing EthoVision software and considered time spent in the reward zone as any time in which the animal has his nose inside the reward port. For quantifying the percentages of trials that a given strategy is used, we considered a trial to be a Seek trial if animals spent time in the reward zone and received shock, an Avoiding trial if it spent 0s in the reward port but did not receive shock, and a Timing trial if animals spent time in the reward port but did not receive shock. Group averages were created and shown from both the time in zones and percent strategies chosen. For each animal, transition matrices were computed using the formula $P_{ij} = n_{ij}N_i$, where P_{ij} represents the probability of transitioning from strategy i to strategy j, nij is the number of transitions from i to j, and Ni is the total number of transitions from strategy i.

Whole-brain-cFos analysis:

Whole-brain cFos density values were obtained for control and experimental groups and all statistical tests related to distributions were performed and plotted using Cumming plots from the DABEST package and Python 3.9 [51]. 95% confidence intervals were calculated for all brain regions from 5000 bootstrap re-samples. Any p-value reported is the probability of observing the effect size (or greater), assuming the null hypothesis of zero difference is true.

Graph network creation:

Whole-brain cFos density for each brain region were averaged across both hemispheres leaving out measured fiber tracts and layer information. Spearman correlation values across regions were calculated from these density metrics across all animals in the respective conditions. We thresholded the correlation matrix keeping only coefficients with a $p < 0.01$. These Spearman correlation coefficients were then used to create a Graph. Graphs were created using Networkx and python 3.9. We defined a Graph (*G*) as a collection of nodes and edges (*N, E*), where *N* is the set of nodes that make up the graph and *E* is the set of edges that connect the nodes, stated as:

G=(N,E),V = {n | n [G},E= {(ei,ej) | (ei,ej) [N ei= ej}

In our Graph objects each brain region represents a node and their pairwise Spearman correlation coefficients represent the edges. We constructed null Graphs by randomly shuffling the edges while preserving the total number of edges each node has. To reduce noise we then subtracted the edge weights in our null Graph from the edges in our real Graph for each condition. If an edge was present in the real Graph but not in the null Graph, the edge was retained with its original weight from the real Graph. Next we subtracted the edges from control Graphs from edges of the experimental Graphs for male and female mice respectively, resulting in Graphs that reflect the unique relationships only present during our experiment. The resulting Graph was then used for further analysis. Networks were plotted using Gephi.In order to identify 'Hubs' we chose four network statistics as done in prior work [18]: *Eigenvector centrality* (i.e., how often a node is connected to highly connected nodes), *Shortest path length* (i.e., average length of the shortest possible path between a node and every other node in the graph), *Clustering coefficient* (i.e., how often a node is connected to another node that forms a local clique), and *Betweenness* (i.e., how often a node is in the shortest path between all pairs of nodes). We considered a node significantly important for a given statistic depending on if they were in the top 20% for *Eigenvector centrality* and *Betweenness* or bottom 20% for *Shortest path length* and *Clustering coefficient* [52]. We considered a hub any node which was significantly important in at least one of these network statistics.

Fiber photometry analysis:

All fiber photometry analysis was performed using the GuPPy pipeline [53]. The data was filtered using a zero-phase moving average linear digital filter of a window of 5 bins for event detection. For event triggered averages we z-scored the entire trace and aggregated all within-animal signals and then marked any bin that exceeds 1.96 z's as a significant peri-event.

Statistical analysis:

Data are presented as mean ± s.e.m. unless otherwise indicated. All data analyses were performed in custom code in Python 3.9 and GraphPad (Prism 9 for Windows, GraphPad Software, San Diego, California USA). Data sets were tested for normality using the Shapiro-Wilk test and analyzed using either t-tests or ordinary one-way ANOVAs for normally distributed data. $P < 0.05$ was considered statistically significant.

Declarations

Acknowledgements:

Declaration of Interest: The authors declare no competing interests.

References

1. Litz B. T., Weathers F. W., Monaco V., Herman D. S., Wulfsohn M., Marx B., et al. (1996). Attention, arousal, and memory in posttraumatic stress disorder. J. Trauma. Stress 9, 497–520.
2. Hayes JP, Vanelzakker MB, Shin LM. Emotion and cognition interactions in PTSD: a review of neurocognitive and neuroimaging studies. Front Integr Neurosci. 2012 Oct 9;6:89. doi: 10.3389/fnint.2012.00089. PMID: 23087624; PMCID: PMC3466464.
3. Verdejo-García A, Pérez-García M, Bechara A. Emotion, decision-making and substance dependence: a somatic-marker model of addiction. Curr Neuropharmacol. 2006 Jan;4(1):17-31. doi: 10.2174/157015906775203057. PMID: 18615136; PMCID: PMC2430678.
4. Zhao Y, Sallie SN, Cui H, Zeng N, Du J, Yuan T, Li D, De Ridder D, Zhang C. Anterior Cingulate Cortex in Addiction: New Insights for Neuromodulation. Neuromodulation. 2020 Oct 9. doi: 10.1111/ner.13291. Epub ahead of print. PMID: 33090660.
5. Young DA, Chao L, Neylan TC, O'Donovan A, Metzler TJ, Inslicht SS. Association among anterior cingulate cortex volume, psychophysiological response, and PTSD diagnosis in a Veteran sample. Neurobiol Learn Mem. 2018 Nov;155:189-196. doi: 10.1016/j.nlm.2018.08.006. Epub 2018 Aug 4. PMID: 30086395; PMCID: PMC6361720.
6. van Heukelum S, Mars RB, Guthrie M, Buitelaar JK, Beckmann CF, Tiesinga PHE, Vogt BA, Glennon JC, Havenith MN. Where is Cingulate Cortex? A Cross-Species View. Trends Neurosci. 2020 May;43(5):285-299. doi: 10.1016/j.tins.2020.03.007. Epub 2020 Apr 10. PMID: 32353333.
7. Kitamura T, Ogawa SK, Roy DS, Okuyama T, Morrissey MD, Smith LM, Redondo RL, Tonegawa S. Engrams and circuits crucial for systems consolidation of a memory. Science. 2017 Apr 7;356(6333):73-78. doi: 10.1126/science.aam6808. PMID: 28386011; PMCID: PMC5493329.
8. Surets M, Caban-Murillo A, Ramirez S. Prelimbic cortex ensembles promote appetitive learning-associated behavior. Learn Mem. 2024 Feb 26;31(1-2):a053892. doi: 10.1101/lm.053892.123. PMID: 38408863; PMCID: PMC10903945.
9. Diehl MM, Bravo-Rivera C, Rodriguez-Romaguera J, Pagan-Rivera PA, Burgos-Robles A, Roman-Ortiz C, Quirk GJ. Active avoidance requires inhibitory signaling in the rodent prelimbic prefrontal cortex. Elife. 2018 May 31;7:e34657. doi: 10.7554/eLife.34657. PMID: 29851381; PMCID: PMC5980229.
10. Gongwer MW, Klune CB, Couto J, Jin B, Enos AS, Chen R, Friedmann D, DeNardo LA. Brain-Wide Projections and Differential Encoding of Prefrontal Neuronal Classes Underlying Learned and Innate Threat Avoidance. J Neurosci. 2023 Aug 9;43(32):5810-5830. doi: 10.1523/JNEUROSCI.0697-23.2023. Epub 2023 Jul 25. PMID: 37491314; PMCID: PMC10423051.
11. Burgos-Robles A, Bravo-Rivera H, Quirk GJ. Prelimbic and infralimbic neurons signal distinct aspects of appetitive instrumental behavior. PLoS One. 2013;8(2):e57575. doi: 10.1371/journal.pone.0057575. Epub 2013 Feb 27. PMID: 23460877; PMCID: PMC3583875.
12. Bercovici DA, Princz-Lebel O, Schumacher JD, Lo VM, Floresco SB. Temporal Dynamics Underlying Prelimbic Prefrontal Cortical Regulation of Action Selection and Outcome Evaluation during Risk/Reward Decision-Making. J Neurosci. 2023 Feb 15;43(7):1238-1255. doi: 10.1523/JNEUROSCI.0802-22.2022. Epub 2023 Jan 6. PMID: 36609453; PMCID: PMC9962784.

13. Josselyn SA, Tonegawa S. Memory engrams: Recalling the past and imagining the future. Science. 2020 Jan 3;367(6473):eaaw4325. doi: 10.1126/science.aaw4325. PMID: 31896692; PMCID: PMC7577560.
14. Ryan TJ, Ortega-de San Luis C, Pezzoli M, Sen S. Engram cell connectivity: an evolving substrate for information storage. Curr Opin Neurobiol. 2021 Apr;67:215-225. doi: 10.1016/j.conb.2021.01.006. Epub 2021 Mar 31. PMID: 33812274.
15. Denny CA, Lebois E, Ramirez S. From Engrams to Pathologies of the Brain. Front Neural Circuits. 2017 Apr 7;11:23. doi: 10.3389/fncir.2017.00023. PMID: 28439228; PMCID: PMC5383718.
16. Suto N, Laque A, De Ness GL, Wagner GE, Watry D, Kerr T, Koya E, Mayford MR, Hope BT, Weiss F. Distinct memory engrams in the infralimbic cortex of rats control opposing environmental actions on a learned behavior. Elife. 2016 Dec 10;5:e21920. doi: 10.7554/eLife.21920. PMID: 27938664; PMCID: PMC5201415.
17. Ramirez S, Liu X, MacDonald CJ, Moffa A, Zhou J, Redondo RL, Tonegawa S. Activating positive memory engrams suppresses depression-like behaviour. Nature. 2015 Jun 18;522(7556):335-9. doi: 10.1038/nature14514. PMID: 26085274; PMCID: PMC5583720.
18. Dorst KE, Senne RA, Diep AH, de Boer AR, Suthard RL, Leblanc H, Ruesch EA, Pyo AY, Skelton S, Carstensen LC, Malmberg S, McKissick OP, Bladon JH, Ramirez S. Hippocampal Engrams Generate Variable Behavioral Responses and Brain-Wide Network States. J Neurosci. 2024 Jan 10;44(2):e0340232023. doi: 10.1523/JNEUROSCI.0340-23.2023. PMID: 38050098; PMCID: PMC10860633.
19. Cummings KA, Bayshtok S, Dong TN, Kenny PJ, Clem RL. Control of fear by discrete prefrontal GABAergic populations encoding valence-specific information. Neuron. 2022 Sep 21;110(18):3036-3052.e5. doi: 10.1016/j.neuron.2022.07.004. Epub 2022 Aug 8. PMID: 35944526; PMCID: PMC10009874.
20. Vetere G, Kenney JW, Tran LM, Xia F, Steadman PE, Parkinson J, Josselyn SA, Frankland PW. Chemogenetic Interrogation of a Brain-wide Fear Memory Network in Mice. Neuron. 2017 Apr 19;94(2):363-374.e4. doi: 10.1016/j.neuron.2017.03.037. PMID: 28426969.
21. Roy DS, Park YG, Kim ME, Zhang Y, Ogawa SK, DiNapoli N, Gu X, Cho JH, Choi H, Kamentsky L, Martin J, Mosto O, Aida T, Chung K, Tonegawa S. Brain-wide mapping reveals that engrams for a single memory are distributed across multiple brain regions. Nat Commun. 2022 Apr 4;13(1):1799. doi: 10.1038/s41467-022-29384-4. PMID: 35379803; PMCID: PMC8980018.
22. Shpokayte M, McKissick O, Guan X, Yuan B, Rahsepar B, Fernandez FR, Ruesch E, Grella SL, White JA, Liu XS, Ramirez S. Hippocampal cells segregate positive and negative engrams. Commun Biol. 2022 Sep 26;5(1):1009. doi: 10.1038/s42003-022-03906-8. PMID: 36163262; PMCID: PMC9512908.
23. Bravo-Rivera H, Rubio Arzola P, Caban-Murillo A, Vélez-Avilés AN, Ayala-Rosario SN, Quirk GJ. Characterizing Different Strategies for Resolving Approach-Avoidance Conflict. Front Neurosci. 2021 Feb 25;15:608922. doi: 10.3389/fnins.2021.608922. PMID: 33716644; PMCID: PMC7947632.

24. Sporns O. Graph theory methods: applications in brain networks. Dialogues Clin Neurosci. 2018 Jun;20(2):111-121. doi: 10.31887/DCNS.2018.20.2/osporns. PMID: 30250388; PMCID: PMC6136126.
25. Rubinov M, Sporns O. Complex network measures of brain connectivity: uses and interpretations. Neuroimage. 2010 Sep;52(3):1059-69. doi: 10.1016/j.neuroimage.2009.10.003. Epub 2009 Oct 9. PMID: 19819337.
26. Stefaniuk M, Pawłowska M, Barański M, Nowicka K, Zieliński Z, Bijoch Ł, Legutko D, Majka P, Bednarek S, Jermakow N, Wójcik D, Kaczmarek L. Global brain c-Fos profiling reveals major functional brain networks rearrangements after alcohol reexposure. Neurobiol Dis. 2023 Mar;178:106006. doi: 10.1016/j.nbd.2023.106006. Epub 2023 Jan 20. PMID: 36682503.
27. Ito R, Lee ACH. The role of the hippocampus in approach-avoidance conflict decision-making: Evidence from rodent and human studies. Behav Brain Res. 2016 Oct 15;313:345-357. doi: 10.1016/j.bbr.2016.07.039. Epub 2016 Jul 25. PMID: 27457133.
28. Schumacher A, Villaruel FR, Ussling A, Riaz S, Lee ACH, Ito R. Ventral Hippocampal CA1 and CA3 Differentially Mediate Learned Approach-Avoidance Conflict Processing. Curr Biol. 2018 Apr 23;28(8):1318-1324.e4. doi: 10.1016/j.cub.2018.03.012. Epub 2018 Apr 5. PMID: 29606418.
29. Grant RI, Doncheck EM, Vollmer KM, Winston KT, Romanova EV, Siegler PN, Holman H, Bowen CW, Otis JM. Specialized coding patterns among dorsomedial prefrontal neuronal ensembles predict conditioned reward seeking. Elife. 2021 Jun 29;10:e65764. doi: 10.7554/eLife.65764. PMID: 34184635; PMCID: PMC8277349.
30. Muysers H, Chen HL, Hahn J, Folschweiller S, Sigurdsson T, Sauer JF, Bartos M. A persistent prefrontal reference frame across time and task rules. Nat Commun. 2024 Mar 8;15(1):2115. doi: 10.1038/s41467-024-46350-4. PMID: 38459033; PMCID: PMC10923947.
31. de Kloet SF, Bruinsma B, Terra H, Heistek TS, Passchier EMJ, van den Berg AR, Luchicchi A, Min R, Pattij T, Mansvelder HD. Bi-directional regulation of cognitive control by distinct prefrontal cortical output neurons to thalamus and striatum. Nat Commun. 2021 Mar 31;12(1):1994. doi: 10.1038/s41467-021-22260-7. PMID: 33790281; PMCID: PMC8012364.
32. Cho KKA, Shi J, Phensy AJ, Turner ML, Sohal VS. Long-range inhibition synchronizes and updates prefrontal task activity. Nature. 2023 May;617(7961):548-554. doi: 10.1038/s41586-023-06012-9. Epub 2023 Apr 26. PMID: 37100905; PMCID: PMC10191848.
33. Zhang Y, Denman AJ, Liang B, Werner CT, Beacher NJ, Chen R, Li Y, Shaham Y, Barbera G, Lin DT. Detailed mapping of behavior reveals the formation of prelimbic neural ensembles across operant learning. Neuron. 2022 Feb 16;110(4):674-685.e6. doi: 10.1016/j.neuron.2021.11.022. Epub 2021 Dec 17. PMID: 34921779; PMCID: PMC8899843.
34. Terra H, Bruinsma B, de Kloet SF, van der Roest M, Pattij T, Mansvelder HD. Prefrontal Cortical Projection Neurons Targeting Dorsomedial Striatum Control Behavioral Inhibition. Curr Biol. 2020 Nov 2;30(21):4188-4200.e5. doi: 10.1016/j.cub.2020.08.031. Epub 2020 Sep 3. PMID: 32888489.

35. Ambroggi F, Ghazizadeh A, Nicola SM, Fields HL. Roles of nucleus accumbens core and shell in incentive-cue responding and behavioral inhibition. J Neurosci. 2011 May 4;31(18):6820-30. doi: 10.1523/JNEUROSCI.6491-10.2011. PMID: 21543612; PMCID: PMC3145462.
36. Suzuki M, Pennartz CMA, Aru J. How deep is the brain? The shallow brain hypothesis. Nat Rev Neurosci. 2023 Dec;24(12):778-791. doi: 10.1038/s41583-023-00756-z. Epub 2023 Oct 27. PMID: 37891398.
37. Grant KA, Newman N, Lynn C, Davenport C, Gonzales S, Cuzon Carlson VC, Kroenke CD. Brain Functional Connectivity Mapping of Behavioral Flexibility in Rhesus Monkeys. J Neurosci. 2022 Jun 15;42(24):4867-4878. doi: 10.1523/JNEUROSCI.0816-21.2022. Epub 2022 May 12. PMID: 35552233; PMCID: PMC9188385.
38. du Plessis KC, Basu S, Rumbell TH, Lucas EK. Sex-Specific Neural Networks of Cued Threat Conditioning: A Pilot Study. Front Syst Neurosci. 2022 May 17;16:832484. doi: 10.3389/fnsys.2022.832484. PMID: 35656357; PMCID: PMC9152023.
39. LaClair M, Febo M, Nephew B, Gervais NJ, Poirier G, Workman K, Chumachenko S, Payne L, Moore MC, King JA, Lacreuse A. Sex Differences in Cognitive Flexibility and Resting Brain Networks in Middle-Aged Marmosets. eNeuro. 2019 Jul 25;6(4):ENEURO.0154-19.2019. doi: 10.1523/ENEURO.0154-19.2019. PMID: 31262949; PMCID: PMC6658914.
40. Anastasiades PG, Carter AG. Circuit organization of the rodent medial prefrontal cortex. Trends Neurosci. 2021 Jul;44(7):550-563. doi: 10.1016/j.tins.2021.03.006. Epub 2021 May 7. PMID: 33972100; PMCID: PMC8222144.
41. Huang Z, Chung M, Tao K, Watarai A, Wang MY, Ito H, Okuyama T. Ventromedial prefrontal neurons represent self-states shaped by vicarious fear in male mice. Nat Commun. 2023 Jul 3;14(1):3458. doi: 10.1038/s41467-023-39081-5. PMID: 37400435; PMCID: PMC10318047.
42. Kyriazi P, Headley DB, Paré D. Different Multidimensional Representations across the Amygdalo-Prefrontal Network during an Approach-Avoidance Task. Neuron. 2020 Aug 19;107(4):717-730.e5. doi: 10.1016/j.neuron.2020.05.039. Epub 2020 Jun 19. PMID: 32562662; PMCID: PMC7442738.
43. Fernandez-Leon JA, Engelke DS, Aquino-Miranda G, Goodson A, Rasheed MN, Do Monte FH. Neural correlates and determinants of approach-avoidance conflict in the prelimbic prefrontal cortex. Elife. 2021 Dec 16;10:e74950. doi: 10.7554/eLife.74950. PMID: 34913438; PMCID: PMC8853658.
44. Masset P, Qin S, Zavatone-Veth JA. Drifting neuronal representations: Bug or feature? Biol Cybern. 2022 Jun;116(3):253-266. doi: 10.1007/s00422-021-00916-3. Epub 2022 Jan 7. PMID: 34993613.
45. Mau W, Hasselmo ME, Cai DJ. The brain in motion: How ensemble fluidity drives memory-updating and flexibility. Elife. 2020 Dec 29;9:e63550. doi: 10.7554/eLife.63550. PMID: 33372892; PMCID: PMC7771967.
46. Choe IH, Byun J, Kim KK, Park S, Kim I, Jeong J, Shin HS. Mice in social conflict show rule-observance behavior enhancing long-term benefit. Nat Commun. 2017 Nov 7;8(1):1176. doi: 10.1038/s41467-017-01091-5. PMID: 29109508; PMCID: PMC5673895.

47. Spröwitz A, Bock J, Braun K. Sex-specific positive and negative consequences of avoidance training during childhood on adult active avoidance learning in mice. Front Behav Neurosci. 2013 Oct 16;7:143. doi: 10.3389/fnbeh.2013.00143. PMID: 24137115; PMCID: PMC3797392.
48. Keiser AA, Turnbull LM, Darian MA, Feldman DE, Song I, Tronson NC. Sex Differences in Context Fear Generalization and Recruitment of Hippocampus and Amygdala during Retrieval. Neuropsychopharmacology. 2017 Jan;42(2):397-407. doi: 10.1038/npp.2016.174. Epub 2016 Aug 31. PMID: 27577601; PMCID: PMC5399239.
49. Piccin A, Courtand G, Contarino A. Morphine reduces the interest for natural rewards. Psychopharmacology (Berl). 2022 Aug;239(8):2407-2419. doi: 10.1007/s00213-022-06131-7. Epub 2022 Apr 8. PMID: 35396673.
50. Nagai Y, Miyakawa N, Takuwa H, Hori Y, Oyama K, Ji B, Takahashi M, Huang XP, Slocum ST, DiBerto JF, Xiong Y, Urushihata T, Hirabayashi T, Fujimoto A, Mimura K, English JG, Liu J, Inoue KI, Kumata K, Seki C, Ono M, Shimojo M, Zhang MR, Tomita Y, Nakahara J, Suhara T, Takada M, Higuchi M, Jin J, Roth BL, Minamimoto T. Deschloroclozapine, a potent and selective chemogenetic actuator enables rapid neuronal and behavioral modulations in mice and monkeys. Nat Neurosci. 2020 Sep;23(9):1157-1167. doi: 10.1038/s41593-020-0661-3. Epub 2020 Jul 6. PMID: 32632286.
51. Ho J, Tumkaya T, Aryal S, Choi H, Claridge-Chang A. Moving beyond P values: data analysis with estimation graphics. Nat Methods. 2019 Jul;16(7):565-566. doi: 10.1038/s41592-019-0470-3. PMID: 31217592.
52. van den Heuvel MP, Mandl RC, Kahn RS, Hulshoff Pol HE. Functionally linked resting-state networks reflect the underlying structural connectivity architecture of the human brain. Hum Brain Mapp. 2009 Oct;30(10):3127-41. doi: 10.1002/hbm.20737. PMID: 19235882; PMCID: PMC6870902.
53. Sherathiya VN, Schaid MD, Seiler JL, Lopez GC, Lerner TN. GuPPy, a Python toolbox for the analysis of fiber photometry data. Sci Rep. 2021 Dec 20;11(1):24212. doi: 10.1038/s41598-021-03626-9. PMID: 34930955; PMCID: PMC8688475.
54. Park YG, Sohn CH, Chen R, McCue M, Yun DH, Drummond GT, Ku T, Evans NB, Oak HC, Trieu W, Choi H, Jin X, Lilascharoen V, Wang J, Truttmann MC, Qi HW, Ploegh HL, Golub TR, Chen SC, Frosch MP, Kulik HJ, Lim BK, Chung K. Protection of tissue physicochemical properties using polyfunctional crosslinkers. Nat Biotechnol. 2018 Dec 17:10.1038/nbt.4281. doi: 10.1038/nbt.4281. Epub ahead of print. PMID: 30556815; PMCID: PMC6579717.

Figures

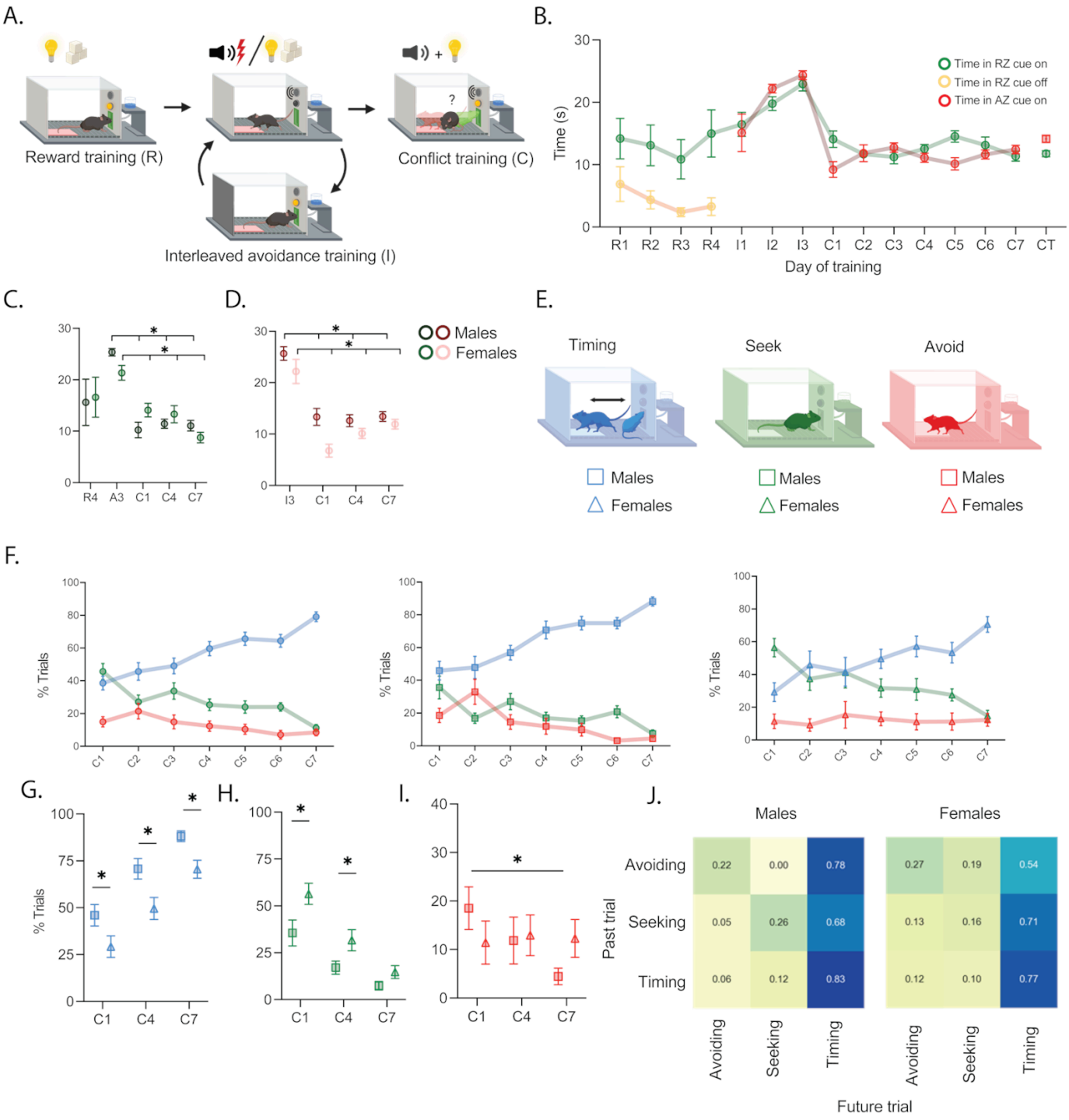

Figure 1

Mice learn to balance reward seeking and punishment avoidance throughout learning. a. First, mice learned to associate a light-cue with reward availability at a nose port (Reward training). Next, mice learned to associate a tone-cue with a shock that can be avoided by stepping into a safe platform. Tone-cue trials were interleaved with light-cue trials (Interleaved avoidance training). Finally, the tone- and light-cue were co-presented in order to create a conflict (Conflict training). b. Time spent poking during

the light-cue (TP-on), outside the light-cue (TP-off), and on the platform during the tone-cue (TA-on) across training days. c. Time spent poking during the light-cue for males and females across training. Multiple comparisons one-way ANOVA. d. Time spent on the platform during the tone-cue for males and females across training. Multiple comparisons one-way ANOVA. e. During conflict trials mice can choose one of three strategies, Avoid (Left) and omit reward, Seek (middle) and receive a shock, or receive less reward and avoid the shock, Timing (Right). f. Percent of trials mice chose a given strategy across conflict training days: All mice (Left), males (Middle), females (Right). g-i. Percent of trials male and female mice chose a given strategy across conflict training. Multiple comparisons one-way ANOVA. j. Probability of choosing a given strategy based on strategy chosen on prior trial. Error bars represent mean ± Standard mean of error (SEM). *$p < 0.05$; males = 12, females = 16.

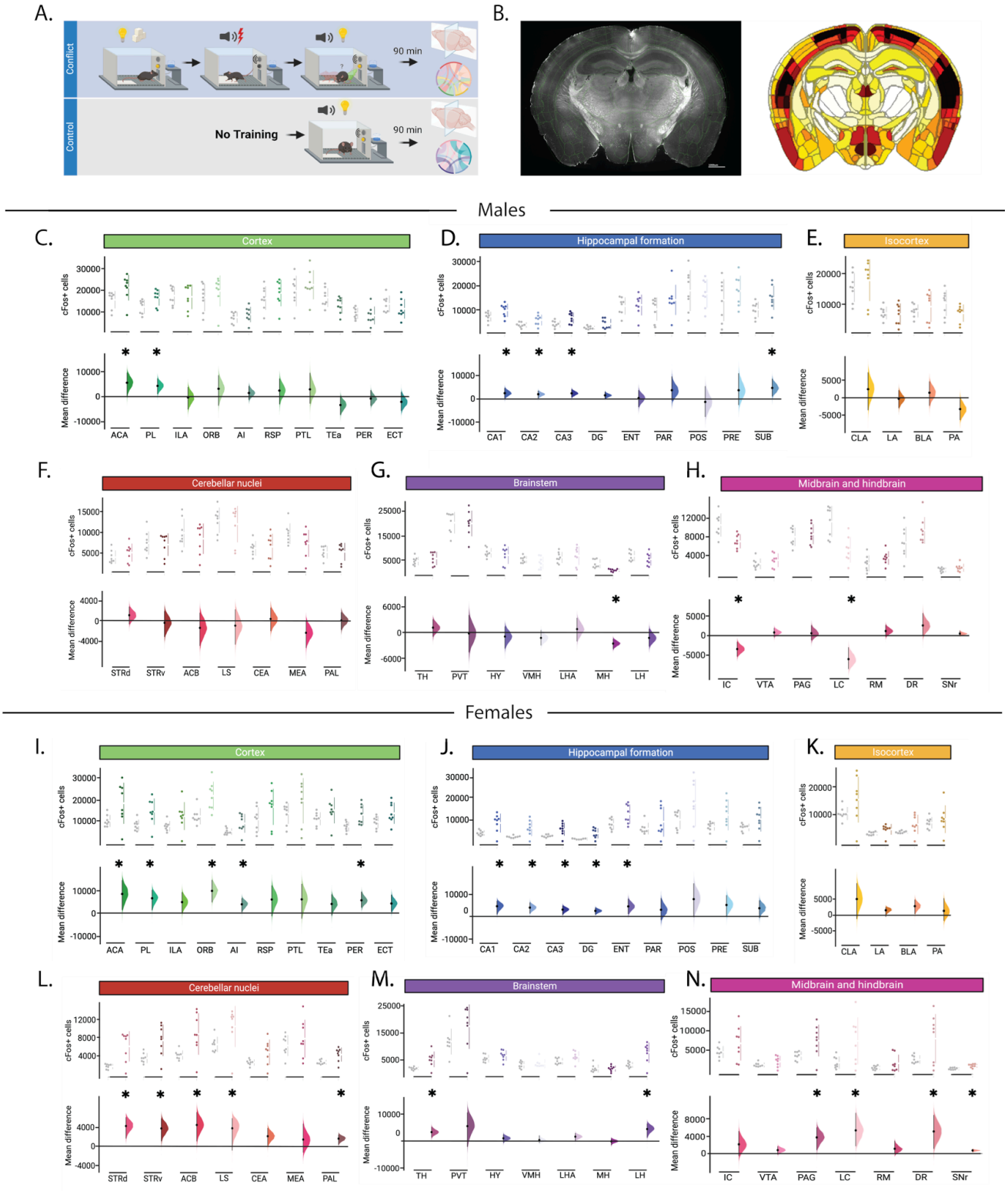

Figure 2

cFos expression profiles during memory-guided conflict resolution. a. Mice underwent training and were sacrificed 90 minutes after the experience. Whole brain clearing and staining was performed after. b. cFos expression density was quantified across all brain regions of cleared brains. c-h. Male cFos densities across a subset of brain regions. i-n. Female cFos densities across a subset of brain regions. For each brain region, the cFos density is presented with a Cumming estimation plot. The top panel

shows the distribution of raw cFos density measures for controls (gray) and experimental mice (color). Each data point represents a single animal. Gapped lines on the right of the raw data points represent the mean (gap) and s.d. (vertical ends) for each group. Bottom panel displays the difference between experimental and control groups, computed from 5,000 bootstrapped re-samples. Per difference distribution: black dot represents the mean; black ticks represent the 95% confidence interval; filled curve represents the sampling error distribution. Student's t-test; *p < 0.05; n = 8 per group.

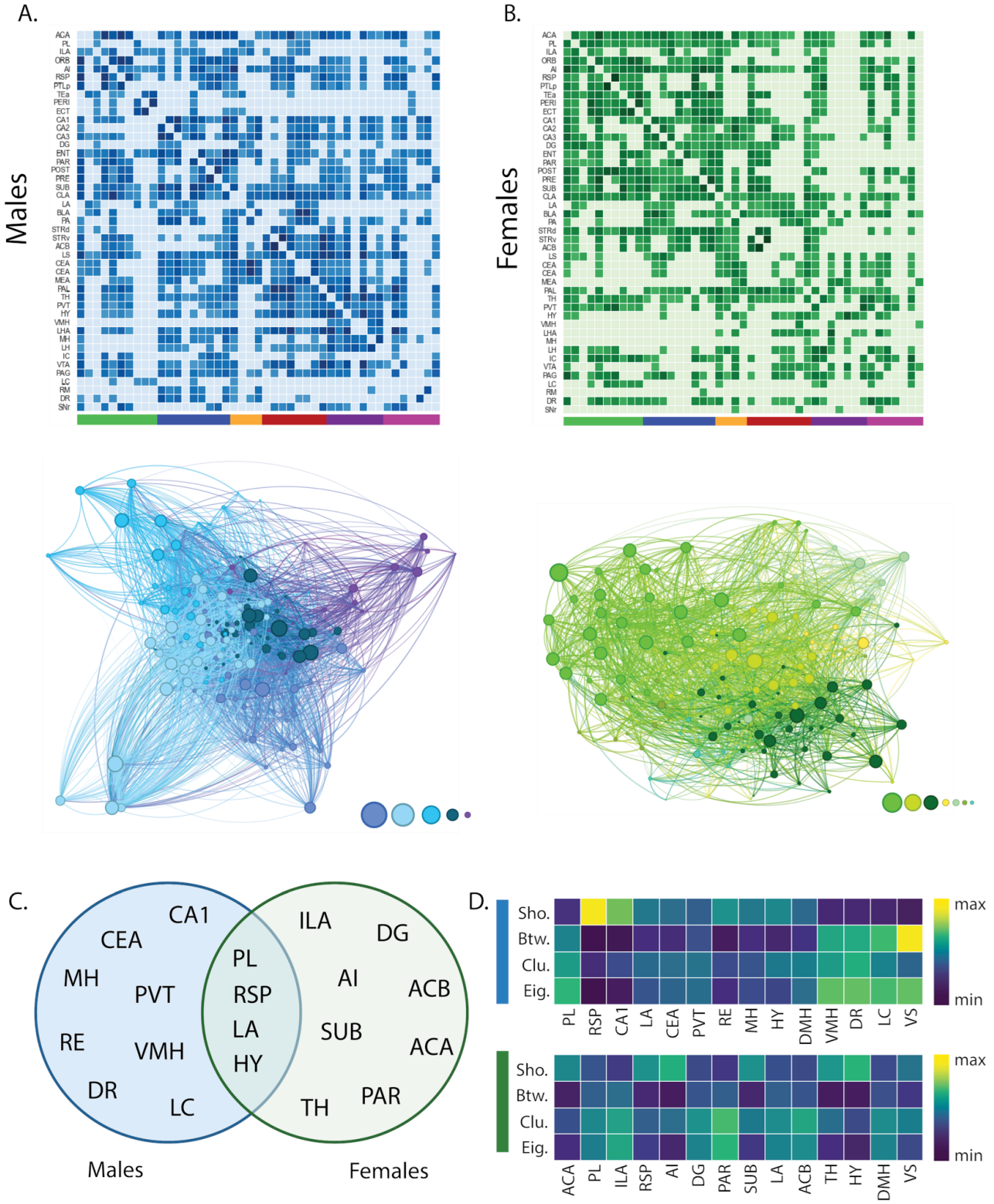

Figure 3

Topological analyses identify hubs recruited during memory-guided conflict resolution. a-b. cFos density correlation matrices organized by regions according to Allen Brain Atlas (top). Based on cFos correlations, graph-based networks were created (bottom) for males and females. Colors represent distinct clusters within each network. Node size represents Eigen centrality value for that node normalized to all other nodes. Relative size and amount of clusters is shown at the bottom as a single color circle per cluster. c. Topological measures used to detect hubs. d. Subset of hubs for male and female networks. e. Relative measures of hub characteristics for a subset of hubs for male and female networks: Sho, shortest path length; Btw, betweenness centrality; Clu, clustering coefficient; Eig, eigen-centrality. Each measure is normalized based on subset maximum and minimum values.

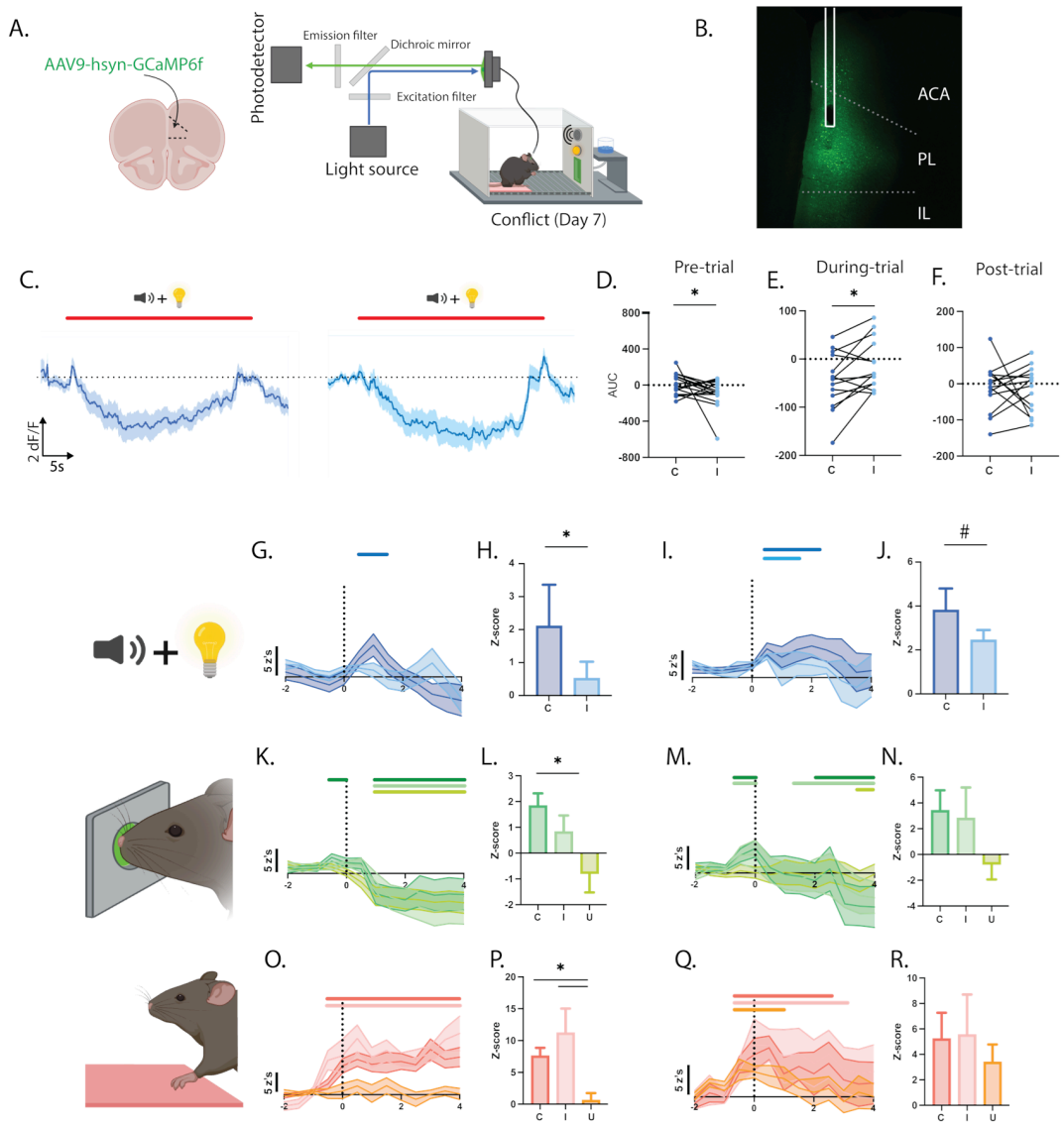

Figure 4

Prelimbic cortex calcium activity signals context and behavior during conflict resolution. a. Fiber photometry recordings of PL neurons during the last day of conflict training. To record calcium activity, mice were injected with AAV9-hsyn-GCaMP6f and received a unilateral optical fiber implant. b. Representative histology of PL expression of AAV9-hsyn-GCaMP6f. c. Average calcium activity across a Timing trial (left) and a Seeking trial (right). Trial period is indicated by the red bar above. 0 dF/F is

denoted by a dashed black line. d. Average AUC of calcium signal during the 15s prior to trial start for Timing and Seeking trials. e. Average AUC of calcium signal during the first 25s of Timing and Seeking trials. f. Average AUC of calcium signal during the 15s post Timing and Seeking trials. g-j. Perievent analysis for calcium activity during the trial-start epoch for males and females. k-n. Perievent analysis for calcium activity during nose-poking epoch for males and females. o-r. Perievent analysis for calcium activity during platform mounting epoch for males and females. Calcium activity traces are represented as z-score %dF/F. Onset of each event is represented in dashed lines. Significant epoch is denoted by the color bar above each trace. Male and female comparisons for cue-onset show the average z-score 1s after cue-onset. Male and female comparisons for nose-poking and platform mounting show the average z-score 1s prior to behavioral epoch. Error bars represent mean ± Standard mean of error (SEM). For perievent analysis: multiple comparisons one-way ANOVA. * $p < 0.05$; males = 10, females = 8.

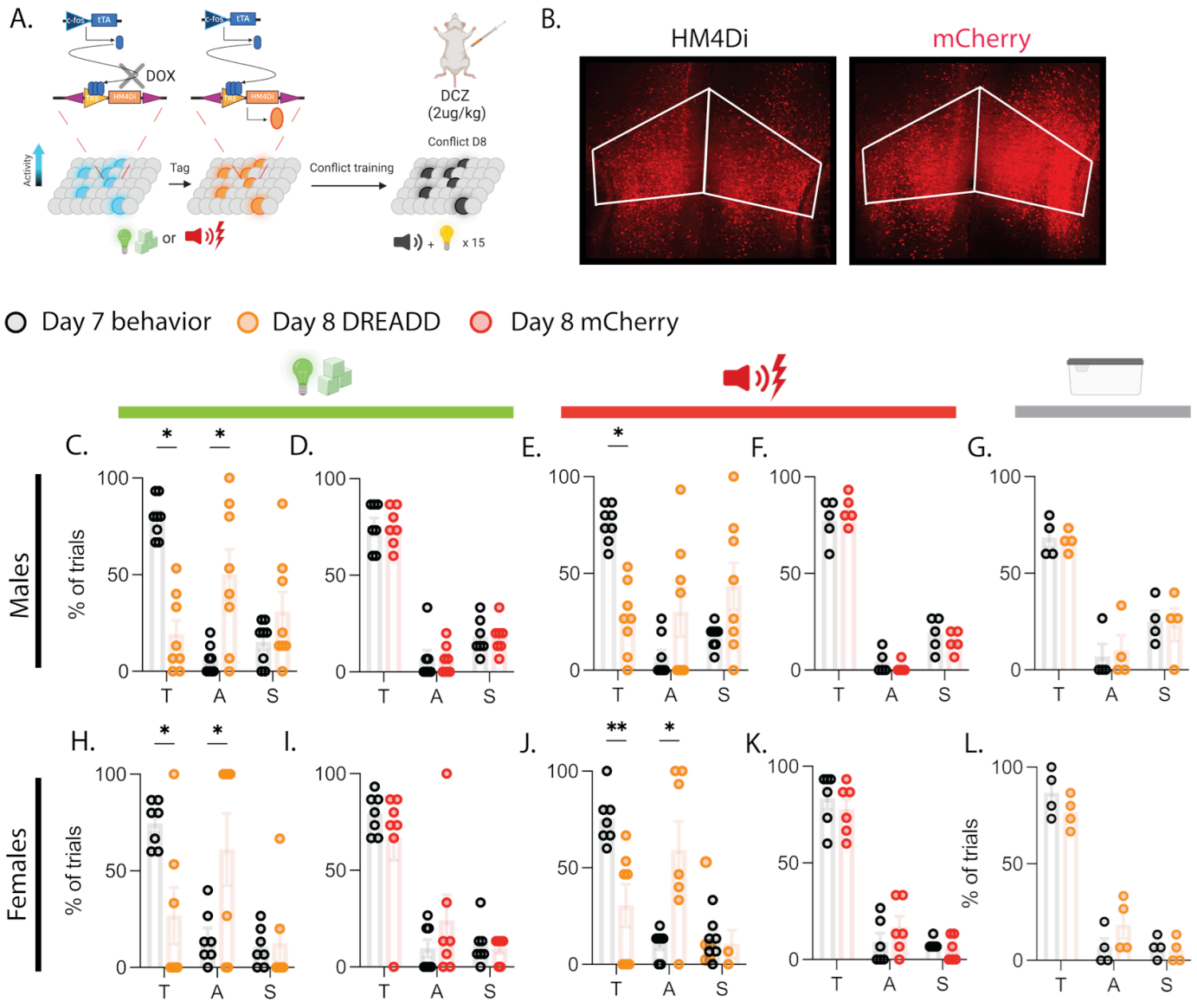

Figure 5

Prelimbic cortex engrams are necessary for memory-guided conflict resolution. a. Mice injected with an activity dependent labeling strategy to express an inhibitory HM4Di in PL. A tagging window was opened during only light-cue presentations or during only tone-cue presentations prior to the start of conflict training in order to label the reward seeking and avoidance engram respectively. After conflict training mice received an additional conflict test day in which DCZ was administered i.p. prior to the start of the session to silence labeled cells. b. Representative histology of PL expression of AAV9-cFos-tTA/ TRE-HM4Di-mCherry. c-l. Percent of trials mice chose a given strategy: Timing (T), Avoiding (A), Seeking (S). Reward tagged group is denoted by green color bar, avoidance tagged group is denoted by red color bar, and neutral cage tagged is denoted by gray color bar. Error bars represent mean ± Standard mean of error (SEM). Paired t-test. * $p < 0.05$; n = 4-8.

Supplementary Files

This is a list of supplementary files associated with this preprint. Click to download.

- Extendeddatafigures.docx